

Full-wave-based transmission-line model for lossy-substrate multiconductor interconnects

Behzad Kordi^{1,*†}, Greg E. Bridges¹, Joe LoVetri¹ and John E. Nordstrom²

¹ *Department of Electrical and Computer Engineering, University of Manitoba, Winnipeg, Manitoba, Canada R3T 5V6*

² *Manitoba HVDC Research Centre, Winnipeg, Manitoba, Canada R3J 3W1*

SUMMARY

A full-wave-based modal analysis is used for simulating a multiconductor coplanar waveguide (CPW) over a selectively etched lossy silicon substrate. Propagating modes, which are similar to the classic ‘common’ and ‘differential’ modes, are extracted, and circuit theory energy relationships are used for the determination of transmission-line model parameters. A time-frequency domain technique is employed for implementing the transmission-line model within a circuit simulator. The model is used to study the effect of etching the dielectric and the substrate for a two-conductor CPW line. The simulation results show that etching both the dielectric and the lossy substrate improves the loss and dispersion characteristics of the CPW line. Copyright © 2007 John Wiley & Sons, Ltd.

Received 27 February 2007; Revised 28 June 2007; Accepted 9 August 2007

KEY WORDS: coplanar transmission line; multiconductor transmission line; coupled transmission line; finite-element method; time-frequency analysis

1. INTRODUCTION

Implementation of transmission-line interconnects on standard low-resistivity Si substrates is becoming more common with the ever-increasing demand to produce high-density, low-cost, and compact wireless communication systems. Coplanar waveguide (CPW) and coplanar stripline configurations are often chosen as the interconnect because of their advantages in circuit layout [1]. Further to their use as on-chip interconnects, these lines can be used, for example, to design filters, power dividers, and electronically controlled phase shifters. However,

*Correspondence to: Behzad Kordi, Department of Electrical and Computer Engineering, University of Manitoba, Winnipeg, Manitoba, Canada R3T 5V6.

†E-mail: bkordi@ee.umanitoba.ca

Contract/grant sponsor: Manitoba Hydro and Natural Sciences and Engineering Research Council of Canada

using Si as the substrate results in high dielectric loss, to an extent where reducing the loss of on-chip passive distributed elements is considered as one of the important challenges in Si-based integrated circuit design [2], and numerous studies have been carried out to understand the loss mechanism for this type of interconnect [3, 4].

One of the common techniques, used to reduce the substrate loss, is to deposit a thin layer of a low-loss dielectric, such as polyimide, between the CPW metallization and Si substrate and construct the CPW on this layer [5]. Further, selective etching of the polyimide (and/or Si) in the slot regions of the CPW has been suggested as a means to improve the dissipative characteristics of the CPW by reducing the effective dielectric constant and redistributing the current density [6, 7]. Other techniques have also been proposed to reduce the loss, for example, using an overlay CPW structure [8].

Various techniques have been proposed for the analysis of metal–insulator–semiconductor transmission lines, especially CPWs and microstrips. Parallel-plate, quasi-static, and quasi-TM approaches, as well as full-wave techniques in conjunction with numerical techniques such as the finite-difference time-domain, the finite-element method (FEM), and the method of moments have been employed (for a brief review see [9]). Multiconductor high-frequency bus architectures pose additional problems [10].

In this paper, a full-wave modal approach is used to analyze a multiconductor CPW transmission line. The finite thickness of conductors is considered and the proximity and skin effects are included. In this technique, an eigenvalue problem is solved using the FEM. For the two-conductor line studied in this paper, two propagating modes are extracted which are similar to the ‘common’ and ‘differential’ modes in classic transmission-line theory. Slow-wave modes are also present that are ignored in the transmission-line approximation. Circuit theory energy relationships are then employed to relate electromagnetic field quantities to the transmission-line circuit model. A circuit model that can be integrated within a circuit simulator is then employed for the time-domain simulation of the lines [11]. This allows the efficient investigation of the effects of coupling and loss in the time domain.

2. THE CPW GEOMETRY

The multiconductor CPW geometries shown in Figure 1 are simulated in this paper. Figure 1(a) shows the original CPW line which is implemented on a low-resistivity Si substrate with a layer of polyimide as the insulating dielectric. The thickness of the Si substrate is 300 μm , with a relative permittivity of $\epsilon_r = 12.1$ and a conductivity of $\sigma = 100 \text{ S/m}$. The thickness of the polyimide layer is 10 μm , and its relative permittivity and conductivity are $\epsilon_r = 2.8$ and $\sigma = 10^{-10} \text{ S/m}$, respectively. The conducting layers are made of gold, with $\sigma = 4.56 \times 10^7 \text{ S/m}$ and their thickness is 1.5 μm . The width of the signal strips is 10 μm . The separation between the strips was chosen to be 8 μm . Figure 1(b) shows the CPW with a self-aligned directional etch of the polyimide using the metal as the mask. In this case, a slot between the signal strips has been etched to see how this will affect the loss. Figure 1(c) shows the CPW with a portion of the Si substrate removed using XeF_2 isotropic etch, forming a suspended CPW. The values of the parameters of the CPW are those typically used in the literature [6].

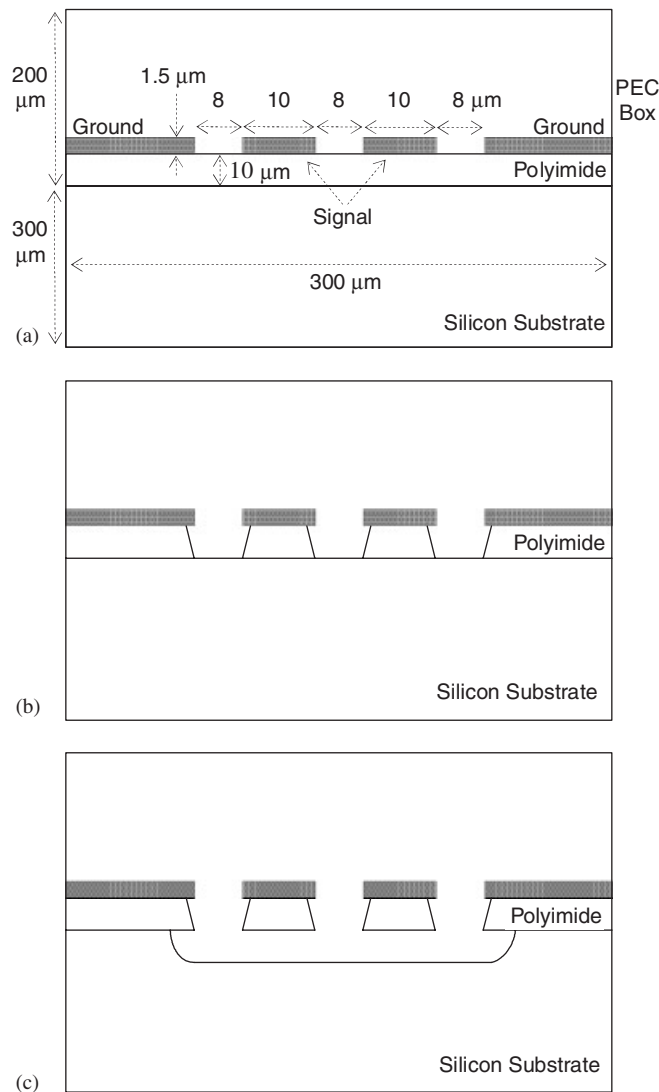


Figure 1. The geometry of a two-conductor CPW line: (a) case 1: no etching; (b) case 2: self-aligned directional etching of the polyimide; and (c) case 3: XeF₂ isotropic etching of the Si substrate that forms a suspended CPW.

3. FULL-WAVE MODAL ANALYSIS

To accurately evaluate the per-unit-length (p.u.l.) parameters of the multiconductor CPW line model, a full-wave analysis is performed where we assume the electromagnetic fields are propagating perpendicular to the transmission-line cross section in the +z direction:

$$\mathbf{E}(x, y, z) = \hat{\mathbf{E}}(x, y) e^{-\gamma z} \tag{1a}$$

$$\mathbf{H}(x, y, z) = \hat{\mathbf{H}}(x, y) e^{-\gamma z} \quad (1b)$$

where $\gamma = \alpha + j\beta$, with α and β being the attenuation and phase constants, respectively. Starting with the wave equation in an inhomogeneous, linear, and isotropic medium,

$$\nabla \times (\mu_r^{-1} \nabla \times \mathbf{E}) - k_0^2 \epsilon_{rc} \mathbf{E} = 0 \quad (2)$$

we can write

$$\nabla_t \times (\mu_r^{-1} \nabla_t \times \mathbf{E}_t) - \mu_r^{-1} \gamma \nabla_t E_z - (k_0^2 \epsilon_{rc} + \mu_r^{-1} \gamma^2) \mathbf{E}_t = 0 \quad (3a)$$

$$-\nabla_t \cdot \mu_r^{-1} \nabla_t E_z - \gamma \nabla_t \cdot (\mu_r^{-1} \mathbf{E}_t) - k_0^2 \epsilon_{rc} E_z = 0 \quad (3b)$$

where $k_0 = \omega(\epsilon_0 \mu_0)^{1/2}$ is the free-space wave number, and

$$\nabla_t \triangleq \frac{\partial}{\partial x} \hat{\mathbf{a}}_x + \frac{\partial}{\partial y} \hat{\mathbf{a}}_y \quad (4a)$$

$$\mathbf{E}_t = E_x \hat{\mathbf{a}}_x + E_y \hat{\mathbf{a}}_y \quad (4b)$$

Note that, in the general transmission-line case, the relative complex permittivity and permeability of the medium may vary over the cross section of the line, i.e. $\epsilon_{rc} = \epsilon_{rc}(x, y)$ and $\mu_r = \mu_r(x, y)$.

With a change of variables using

$$\mathbf{e}_t = -j\gamma \mathbf{E}_t \quad (5a)$$

$$e_z = -jk_0 E_z \quad (5b)$$

Equations (3a) and (3b) become the eigenvalue problem:

$$\nabla_t \times (\mu_r^{-1} \nabla_t \times \mathbf{e}_t) - k_0^2 \epsilon_{rc} \mathbf{e}_t = \mu_r^{-1} \gamma^2 \left(\nabla_t \frac{e_z}{k_0} + \mathbf{e}_t \right) \quad (6a)$$

$$\nabla_t \cdot \mu_r^{-1} \left(\nabla_t \frac{e_z}{k_0} + \mathbf{e}_t \right) + k_0 \epsilon_{rc} e_z = 0 \quad (6b)$$

which is solved using an FEM [12]. The propagating-wave solutions consist of different modes, each having a specific electromagnetic field profile. Among these modes, there are two modes that we identify as ‘common’ and ‘differential’ modes (as the CPW shown in Figure 1 is considered to be a two-conductor transmission line).

For the examples considered in this paper, Equations (6a) and (6b) are solved for frequencies in the range of 0.02–40 GHz, where the cross-sectional dimensions are still much smaller than the smallest transverse wavelength. At frequencies lower than 0.02 GHz, the eigenvalues are very small and very close to each other, thus making mode extraction difficult.

Using the full-wave modal analysis of the multiconductor CPW, both the proximity and skin effects in the conductors are considered. For example, for case 1 in Figure 1(a), the absolute

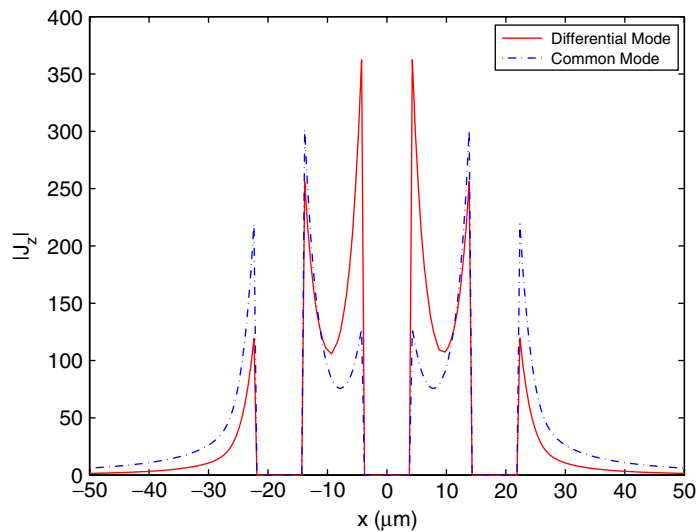


Figure 2. Absolute value of the conduction current density along a horizontal line that passes through the center of the conductors at 5 GHz (for the CPW line shown in Figure 1(a)).

value of the conduction current density, $J_z = \sigma E_z$, along a horizontal line that passes through the center of the conductors is shown in Figure 2 at 5 GHz. The phase of the current density varies over the strips; however, the total currents of the strips are in phase for the common mode and out of phase for the differential mode. The proximity effect causes the current density to be higher at the near edges of the signal strips for the differential mode and at the far edges of the signal strips for the common mode.

The effect of etching on the attenuation and phase constants as a function of frequency is shown in Figure 3. The phase constant is given in terms of the normalized wavelength (normalized to the free-space wavelength). As seen in this figure, etching the dielectric and the substrate significantly decreases the common-mode attenuation constant. For cases 1 and 2, the common-mode attenuation constant is larger than that of the differential mode for higher frequencies, whereas for case 3, the common mode always has a lower attenuation constant. Further, as a result of etching, the fields are concentrated mostly in air which makes the propagation speed closer to that of light. Reduction of loss and similarity of phase constants reduce the dispersive effects of the line.

4. TRANSMISSION-LINE PARAMETERS EXTRACTION

Examining the transverse and normal components (with respect to the line cross section) of the fields over the cross section (except for the metal strips) of the CPW shows that the quasi-TEM assumption is relatively valid even at 40 GHz. Thus, a transmission-line-based model, which can be easily integrated within a circuit simulator, is acceptable for the analysis of these interconnects. The first problem is to extract the p.u.l. parameters of the line which is performed using the circuit theory energy relationships.

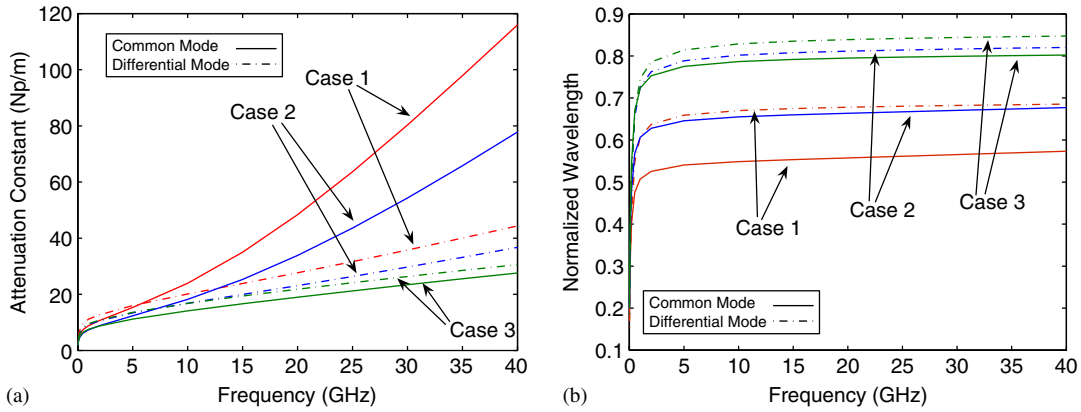


Figure 3. Attenuation constant (a) and normalized wavelength (b) as a function of frequency for the cases shown in Figure 1.

4.1. Parameter extraction using circuit theory energy relationships

Using the fields from the full-wave model, the stored electric and magnetic energy associated with a mode can be approximated with a good accuracy using the transverse field components as

$$W_E = \frac{1}{2} \int_S \epsilon (|E_x|^2 + |E_y|^2) ds \quad (7a)$$

$$W_M = \frac{1}{2} \int_S \mu (|H_x|^2 + |H_y|^2) ds \quad (7b)$$

which are related to the p.u.l. capacitance matrix, \mathbf{C} , and inductance matrix, \mathbf{L} , by

$$W_E = \frac{1}{2} \mathbf{V}^T \mathbf{C} \mathbf{V} \quad (8a)$$

$$W_M = \frac{1}{2} \mathbf{I}^T \mathbf{L} \mathbf{I} \quad (8b)$$

In (8), \mathbf{V} and \mathbf{I} are the line voltage and current vectors, respectively, and T represents complex conjugate transpose. The line ‘current’ and ‘voltage’ used in this equation are obtained by the surface integral of the normal component of the total current density over the signal strips and the line integral of the electric field between the strips, respectively. Equating (7a) with (8a) for each mode, we obtain a set of two equations in two unknowns, whose solution will provide the elements of the capacitance matrix.[‡] Using a similar procedure, one can determine the elements of the inductance matrix using (7b) and (8b).

As there are two loss components (series resistance \mathbf{R} and shunt conductance \mathbf{G}) in the transmission-line model, we assign the resistive loss due to the normal component of the electric field to \mathbf{R} and the resistive loss due to the transverse component of the electric

[‡] Because of symmetry, $C_{11} = C_{22}$, and reciprocity implies that $C_{12} = C_{21}$.

field to \mathbf{G}

$$W_R = \int_S \sigma |E_z|^2 ds \tag{9a}$$

$$W_G = \int_S \sigma (|E_x|^2 + |E_y|^2) ds \tag{9b}$$

The circuit loss components are then evaluated by equating (9a) and (10a) and (9b) and (10b) for each mode, respectively, where

$$W_R = \mathbf{I}^T * \mathbf{R} \mathbf{I} \tag{10a}$$

$$W_G = \mathbf{V}^T * \mathbf{G} \mathbf{V} \tag{10b}$$

Plots of the p.u.l. parameters of the CPW are shown in Figures 4 and 5. A close study of these figures reveals that etching the dielectric reduces the capacitance and the conductance, whereas the inductance and the resistance are not affected. However, etching the substrate lowers the inductance and the resistance and significantly reduces the conductance that results from a modification of the current distribution in the substrate. The capacitance does not change significantly as a result of etching the substrate.

4.2. Accuracy of the approach

In order to verify the accuracy of the circuit parameters extracted using energy relationships and the assumptions made in the previous section, one can re-calculate the modal attenuation and phase constants using the p.u.l. parameters. Given \mathbf{R} , \mathbf{L} , \mathbf{G} , and \mathbf{C} matrices, first we calculate the p.u.l. series impedance and shunt admittance matrices:

$$\mathbf{Z} = \mathbf{R} + j\omega\mathbf{L} \tag{11a}$$

$$\mathbf{Y} = \mathbf{G} + j\omega\mathbf{C} \tag{11b}$$

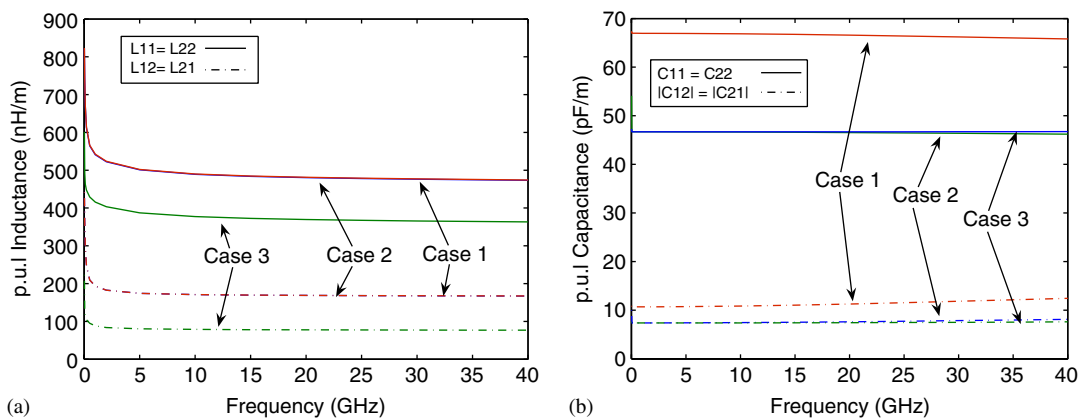


Figure 4. Components of the p.u.l. inductance (a) and capacitance (b) matrices for the cases shown in Figure 1.

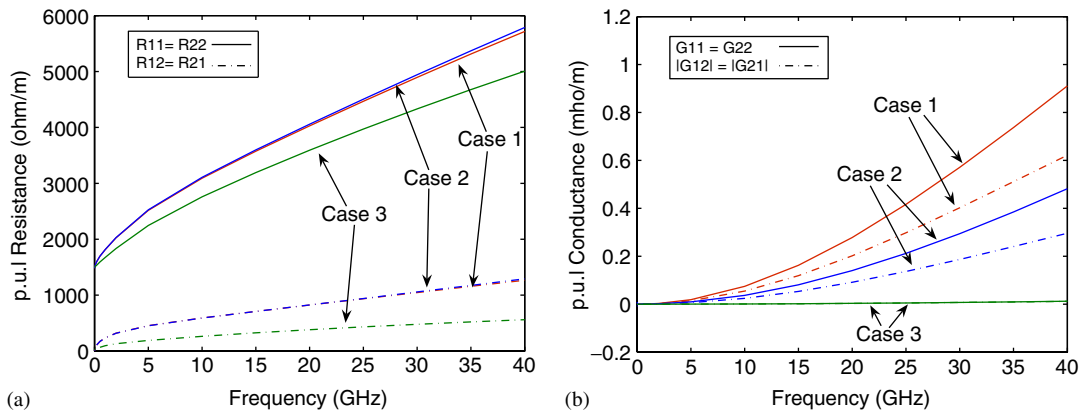


Figure 5. Components of the p.u.l. resistance (a) and conductance (b) matrices for the cases shown in Figure 1.

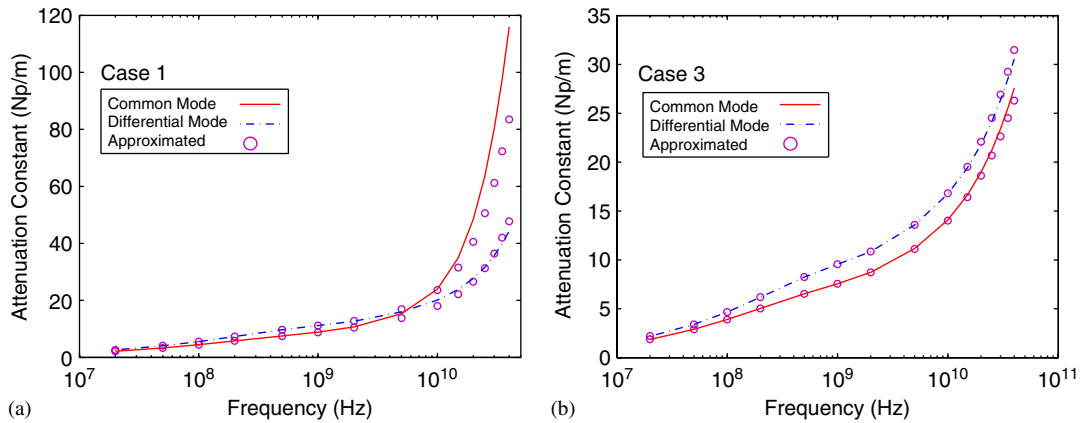


Figure 6. The full-wave and approximated attenuation constant calculated for (a) case 1 and (b) case 3.

The mode-domain propagation constant matrix is calculated using [13]

$$\gamma^2 = \mathbf{T}^{-1} \mathbf{YZT} \tag{12}$$

where \mathbf{T} is a similarity transformation used to diagonalize the \mathbf{YZ} matrix and consists of the eigenvectors of this matrix.

Figures 6 and 7 present a comparison between the attenuation and the propagation constants already plotted in Figure 3 and those calculated using (12). In case 1 (Figure 6(a)), where neither the dielectric nor the substrate is etched, a difference between the full-wave common-mode attenuation constant and that re-calculated using (11) and (12) is observed for frequencies higher than 10 GHz. The difference is about 25% at 40 GHz. The reason for this discrepancy is that in our approximation the loss associated with the resistance matrix, \mathbf{R} , is related to the longitudinal current flowing only through the conductors. However, in the common mode of

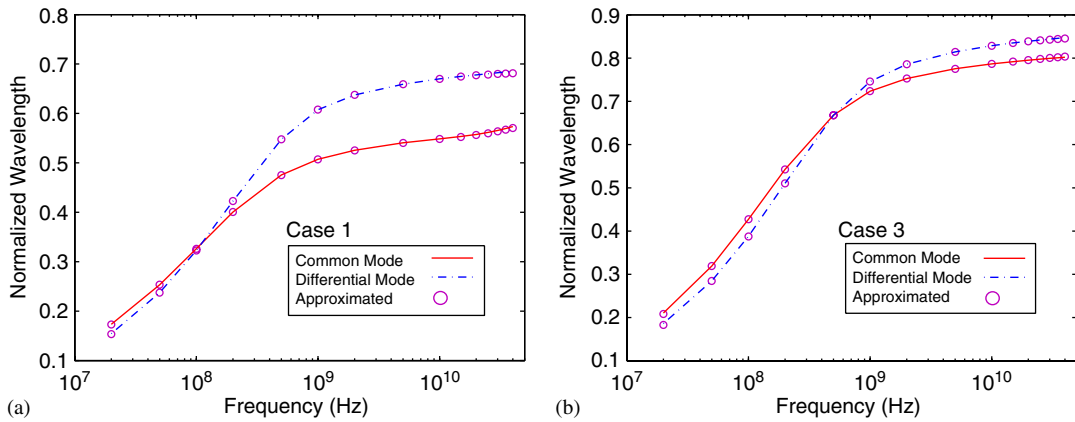


Figure 7. The full-wave and approximated normalized wavelength calculated for (a) case 1 and (b) case 3.

case 1, the longitudinal conduction current in the substrate is also significant, but it is not considered in the calculation of the transmission-line-theory current. In other cases, a very good agreement is observed between the approximated and the full-wave attenuation and phase constants.

5. TIME-DOMAIN SIMULATION RESULTS

Once the variation of the transmission-line parameters with frequency is determined, we employ a model that allows the integration of the transmission line within a time-domain circuit simulator. A fundamental difficulty encountered in integrating transmission-line simulation into a transient circuit simulator arises because network nonlinearities and/or time-dependent components require a time domain analysis, whereas transmission-line characteristics, such as conductor loss and dispersion, are best described in the frequency domain. The issue of mixed time–frequency modeling of lossy coupled multiconductor transmission lines has been studied for many years and various techniques have been resulted (for a brief review see [11]).

In this paper, we use a reduced macro-model where the elements of the propagation matrix, $\mathbf{H}(s) = \exp(-\sqrt{\mathbf{Y}(s)\mathbf{Z}(s)}\ell)$, ℓ being the length of the line, are approximated as [14]

$$H_{ij}(s) = \sum_{k=1}^n \sum_{m=1}^{N_k} \frac{(C_{mk})_{ij}}{s - p_{mk}} e^{-s\tau_k} \tag{13}$$

Here, N_k is the number of poles chosen to approximate the k th mode and n is the number of modes. The poles, p_{mk} and residues, $(C_{mk})_{ij}$, are determined using the Vector Fitting algorithm [15]. The characteristic admittance, $\mathbf{Y}_C(s) = \sqrt{\mathbf{Y}(s)\mathbf{Z}(s)\mathbf{Z}^{-1}(s)}$, is also approximated using a similar approach [14].

With this time-domain analysis approach, the effects of substrate etching on transients and mutual coupling can be efficiently investigated. Figure 8(a) shows the circuit schematic of the

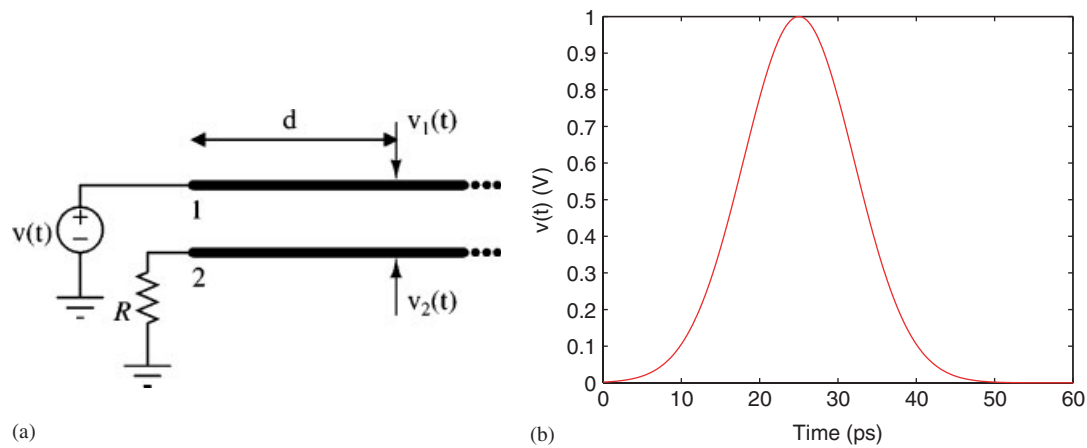


Figure 8. (a) Circuit representation of the two-conductor CPW line. (b) The excitation Gaussian waveform, $v(t)$, whose spectrum is greater than 20% of its maximum for up to 40 GHz.

two-conductor CPW line (whose parameters have already been determined) where one of the conductors is excited by a Gaussian waveform, as shown in Figure 8(b), and the other conductor is terminated with a resistor R . The length of the transmission line is chosen long enough so that reflections are not present at the observation point. The risetime of the Gaussian waveform has been chosen so that the spectrum of the waveform covers the frequency range of interest, i.e. up to 40 GHz.

Simulated waveforms at a distance of $d = 1.5$ cm from the source are shown in Figure 9, for both lines 1 and 2. The waveforms shown in this figure have been calculated for $R = 0$; however, varying R from a short circuit to an open circuit does not significantly change the waveforms on both lines. Figure 9(a) shows that the Gaussian waveform suffers from both dispersion and attenuation; its amplitude is reduced almost to half, and the risetime and the width of the pulse have increased significantly. (For case 1, the attenuation should be even greater since the attenuation constant is underestimated as shown in Figure 6(a).) Etching the polyimide and the substrate dramatically helps to reduce substrate loss effects, whereas etching the polyimide alone does not help as much. Etching also reduces the crosstalk between the lines, as shown in Figure 9(b). The amplitude of the induced waveform in line 2 significantly decreases as a result of etching. Note that etching the polyimide reduces the mutual capacitance and does not affect the mutual inductance, whereas etching both polyimide and the substrate reduces the mutual inductance as well. As a result, case 3 (etching both polyimide and the substrate) shows a lower coupling between lines.

A quantitative study of the effects of etching, resulting from the time-domain simulation of the CPW line, is presented in Table I. The Gaussian excitation waveform has a 10–90% risetime and a full-width at half-maximum (FWHM) of 11.9 and 16.6 ps, respectively, which, as a result of dispersion, are increased by a factor of almost two at the observation point. The terminating resistance R does not have a significant effect on these values. Etching the polyimide alone results in a risetime degradation of 70%, whereas etching both polyimide and the substrate results in a degradation of only 10%.

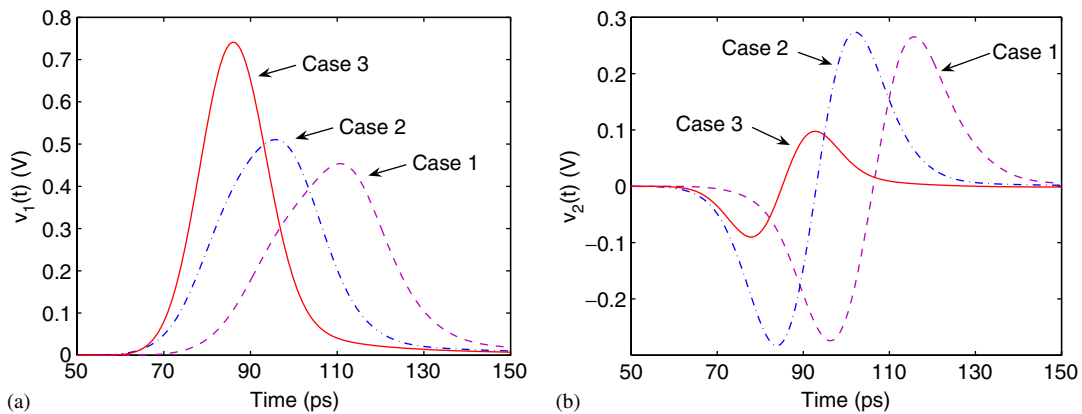


Figure 9. Voltage waveforms at $d = 1.5$ cm from the source on (a) line 1 and (b) line 2 for $R = 0$. The waveforms for other values of R are not significantly different (see Figure 8).

Table I. Risetime (10–90%), full-width at half-maximum (FWHM), and relative amplitude of the voltage on line 1 for the three cases shown in Figure 1 for different values of resistor R (see Figure 8).

	Excitation waveform	$R = 0$			$R = 50 \Omega$			$R = \infty$		
		Case 1	Case 2	Case 3	Case 1	Case 2	Case 3	Case 1	Case 2	Case 3
Risetime (ps)	11.9	23.8	19.4	12.8	24.6	20.4	12.8	24.7	21.0	12.8
FWHM (ps)	16.6	30.5	27.9	18.3	28.8	27.0	18.3	25.5	24.8	18.3
Amplitude	1	0.454	0.511	0.741	0.474	0.525	0.743	0.509	0.558	0.746

6. CONCLUSION

In this paper, a full-wave approach based on modal analysis was used to determine the propagation characteristics of electromagnetic waves in multiconductor CPWs over lossy substrate. This technique was applied to investigate the effects of etching the dielectric insulator and the lossy Si substrate and reveals how etching can improve the loss and dispersion characteristics of the line. Circuit theory energy relationships were used to extract the transmission-line model parameters. To investigate the effects of etching on the transient signals propagating on the line, a reduced-order macro-model was employed. The simulation results show that etching both the dielectric and the substrate significantly reduces the loss and dispersion.

ACKNOWLEDGEMENTS

The authors wish to acknowledge the support of Manitoba Hydro and Natural Sciences and Engineering Research Council of Canada.

REFERENCES

1. Leung LLW, Hon W-C, Chen KJ. Low-loss coplanar waveguides interconnects on low-resistivity silicon substrate. *IEEE Transactions on Components and Packaging Technologies* 2004; **27**(3):507–512.
2. Komijani A, Natarajan A, Hajimiri A. A 24-GHz +14.5-dB fully integrated power amplifier in 0.18- μm CMOS. *IEEE Journal of Solid-State Circuits* 2005; **40**(9):1901–1908.
3. Lederer D, Raskin J-P. Substrate loss mechanisms for microstrip and CPW transmission lines on lossy silicon wafers. *IEEE International Microwave Theory and Techniques Symposium*, Seattle, WA, June 2002.
4. Weisshaar A, Luoh A. Closed-form expressions for the series impedance parameters of on-chip interconnects on multilayer silicon substrates. *IEEE Transactions on Advanced Packaging* 2004; **27**(1):126–134.
5. Suematsu N, Ono M, Kubo S, Iyama Y, Ishida O. L-band internally matched Si-MMIC front end. *IEEE Transactions on Microwave Theory and Techniques* 1996; **44**(12):2375–2378.
6. Ponchak GE, Margomenos A, Katehi LPB. Low-loss CPW on low-resistivity Si substrate with a micromachined polyimide interface layer for RFIC interconnects. *IEEE Transactions on Microwave Theory and Techniques* 2001; **49**(5):866–870.
7. Herrick KJ, Schwarz TA, Katehi LPB. Si-micromachined coplanar waveguides for use in high-frequency circuits. *IEEE Transactions on Microwave Theory and Techniques* 1998; **46**(6):762–768.
8. Kim H-T, Jung S, Park J-H, Baek C-W, Kim Y-K, Kwon Y. A new micromachined overlay CPW structure with low attenuation over wide impedance ranges and its application to low-pass filters. *IEEE Transactions on Microwave Theory and Techniques* 2001; **49**(9):1634–1639.
9. Plaza G, Marqués R, Medina F. Quasi-TM MoL/MoM approach for computing the transmission-line parameters of lossy lines. *IEEE Transactions on Microwave Theory and Techniques* 2006; **54**(1):198–209.
10. Papapolymerou J, Ponchak GE, Dalton E, Bacon A, Tentzeris MM. Crosstalk between finite ground coplanar waveguides over polyimide layers for 3-D MMICs on Si Substrates. *IEEE Transactions on Microwave Theory and Techniques* 2004; **52**(4):1292–1301.
11. Kordi B, LoVetri J, Bridges GE. Finite-difference analysis of dispersive transmission lines within a circuit simulator. *IEEE Transactions on Power Delivery* 2006; **21**(1):234–242.
12. *Comsol Multiphysics User's Manual*. Comsol Inc., 2006.
13. Paul CR. *Analysis of Multiconductor Transmission Lines*. Wiley: New York, 1994.
14. Morched A, Gustavsen B, Tartibi M. A universal model for accurate calculation of electromagnetic transients on overhead and underground cables. *IEEE Transactions on Power Delivery* 1999; **14**(3):1032–1038.
15. Gustavsen B, Semlyen A. Rational approximation of frequency-domain responses by Vector Fitting. *IEEE Transactions on Power Delivery* 1999; **14**(3):1052–1061.

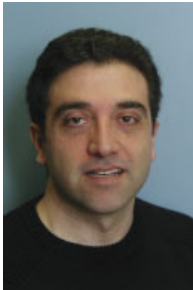
AUTHORS' BIOGRAPHIES



Behzad Kordi received the BSc (with distinction), MSc and PhD degrees all in Electrical Engineering from Amirkabir University of Technology (Tehran Polytechnic), Tehran, Iran, in 1992, 1995, and 2000, respectively. During 1998 and 1999, he was with the Lightning Studies Group at the University of Toronto, Canada, where he was awarded a Graduate Research Grant by the Electrical and Computer Engineering Department of the University of Toronto. In 2002, he joined the Electrical and Computer Engineering Department, University of Manitoba, as a Post-doctoral Fellow where he is currently an Assistant Professor. His research interests concern computational electromagnetics, electromagnetic compatibility (EMC), time-domain simulation of interconnects and transmission lines, and electromagnetic probes. Dr Kordi is the author/coauthor of more than 30 scientific papers published in reviewed journals or presented at international conferences.



Greg E. Bridges received the BSc, MSc and PhD degrees in Electrical Engineering from the University of Manitoba, Canada, in 1982, 1984, and 1989, respectively. He joined the Department of Electrical and Computer Engineering, University of Manitoba, in 1989, where he is currently a Professor. In 1996 he was a visiting scientist at the Communications Research Centre, Ottawa. He is currently the Principal Investigator for the Advanced RF Systems Lab of the National Microelectronics and Photonics Test Collaboratory. He has authored or coauthored publications in the areas of computational electromagnetics and microwave measurement techniques and he holds several patents related to RFIC probing. His research involves computational electromagnetics, RF sensors, and the development of nanoprobe based measurement techniques for high-frequency microelectronics test.



Joe LoVetri received the PhD degree in Electrical Engineering from the University of Ottawa in 1991. From 1991 to 1999, he was an Associate Professor in the Department of Electrical and Computer Engineering, The University of Western Ontario. He is currently a Professor in the Department of Electrical and Computer Engineering and Associate Dean (Research and Graduate Programs) of the Faculty of Engineering, at The University of Manitoba. His main research interests are in time-domain CEM, modeling of EMC problems, GPR, and inverse imaging techniques.



John E. Nordstrom was born in Ottawa, Canada, in 1970. He moved to Thunder Bay, Canada, shortly thereafter, where he eventually received his B.Eng. in Electrical Engineering from Lakehead University in 1997. Since 1998, he has been employed at the Manitoba HVDC Research Centre Inc., where he is currently a developer of the PSCAD simulation software — specifically the transmission lines and load flow solution engines. He received his Masters of Science from the University of Manitoba 2004.